Surface Rebound of Relativistic Dislocations Directly and Efficiently Initiates Deformation Twinning

Qing-Jie Li,[1] Ju Li,[2,*] Zhi-Wei Shan,[3,†] and Evan Ma[1,‡]
[1]Department of Materials Science and Engineering, Johns Hopkins University, Baltimore, Maryland 21218, USA
[2]Department of Nuclear Science and Engineering and Department of Materials Science and Engineering, Massachusetts Institute of Technology, 77 Massachusetts Avenue, Cambridge, Massachusetts 02139, USA
[3]Center for Advancing Materials Performance from the Nanoscale (CAMP-Nano) & Hysitron Applied Research Center in China (HARCC), State Key Laboratory for Mechanical Behavior of Materials, Xi'an Jiaotong University, Xi'an 710049, China
(Received 24 June 2016; revised manuscript received 19 August 2016; published 11 October 2016)

Under ultrahigh stresses (e.g., under high strain rates or in small-volume metals) deformation twinning (DT) initiates on a very short time scale, indicating strong spatial-temporal correlations in dislocation dynamics. Using atomistic simulations, here we demonstrate that surface rebound of relativistic dislocations directly and efficiently triggers DT under a wide range of laboratory experimental conditions. Because of its stronger temporal correlation, surface rebound sustained relay of partial dislocations is shown to be dominant over the conventional mechanism of thermally activated nucleation of twinning dislocations.

DOI: 10.1103/PhysRevLett.117.165501

Recent advances in small-volume materials fabrication have created a remarkable category of metallic crystals that can retain pristine crystal structures on the length scale of $10^1 - 10^2$ nanometers [1–7]. Deformation twinning (DT) has been shown to initiate in these metals at ultrahigh stresses ($\sim 10^{-2}G$, where G is shear modulus) and on a very short time scale ($\ll 0.01$ s, the typical time resolution of state-of-the-art *in situ* microscopy imaging techniques) [2,4–6], indicating strong spatial-temporal correlations in the underlying dislocation dynamics. Such strongly correlated DT mode requires extremely stringent spatial and temporal coordination of twinning dislocations (the right type of partial dislocations on *consecutive* atomic planes one after another [8]). This is hardly possible by the conventional pole mechanism [9,10] due to the pristine nature of the deformation volume, nor by the generally believed thermally activated nucleation (TAN) [2,5–7,11–13] due to possible long waiting time.

In the following, we illustrate that while the first dislocation to initiate DT must come from a TAN event, subsequent twinning dislocations can be generated by dislocations running at speeds near the transverse sound speed (c_t). Specifically, twinning dislocations are generated successively on each and every consecutive atomic plane by a surface-rebound sustained (SRS) nucleation process, in a domino cascade fashion. This mechanism is highly efficient due to its strong temporal correlation; i.e., there is almost no time delay between two successive twinning partials. The SRS mechanism can thus dominate over the TAN mechanism over a wide range of experimental conditions.

Atomistic simulations, reaction pathway sampling method, and the harmonic transition state theory will be combined to reveal the mechanism underlying the strongly correlated DT. Direct molecular dynamics (MD) simulations were performed to observe how dislocations behave after nucleation in highly stressed nanowires and slab configurations. The free end nudged elastic band method (FENEB) [11,14] was used to obtain the activation energy barriers for TAN of surface dislocation. The empirical potential for copper [15] based on the embedded atom method was used to describe the interatomic interactions. All simulations were performed using the LAMMPS package [16] and the results were visualized by the AtomEye [17] and DXA packages [18]. See Ref. [19] for more details on simulation methods.

Figure 1 shows DT initiation in MD simulation of a 10 nm wide [100] oriented square nanowire compressed at 300 K with a strain rate of 10^6 s^{-1} (0.0 ps). The first dislocation was nucleated when the sample-wide axial stress reached ~2.5 GPa [21], and glided across the nanowire (5.5 ps). However, instead of TAN of twinning dislocations, the subsequent DT proceeded via repeated surface rebounds. Specifically, when an incident partial dislocation impacted on a free surface and annihilated, new partial dislocations were *immediately* generated (5.5 → 8.0 ps). The new partials are on neighboring slip planes because of the lack of $\mathbf{b}_p \leftrightarrow -\mathbf{b}_p$ symmetry on the same slip plane (the atoms in the two atomic layers would otherwise sit or slide on top of each other) in face-centered cubic (fcc) metals. The rebounded partials are thus naturally twinning dislocations, which are then accelerated again to high speeds under τ, towards the surface on the other side of the sample (12.0 ps), where another collision kicks out more twinning partials that continue the relay (14. 0 ps). Such SRS relay continued until the sample-wide axial stress (σ) was relaxed to a much lower level of 0.75 GPa (17.0 → 60.0 ps) [21]. The whole DT initiation process was accomplished within 60 ps with a 9-layers twin nucleus (60.0 ps). See Ref. [22] for more details and Ref. [23] for similar DT initiation in a [110] oriented

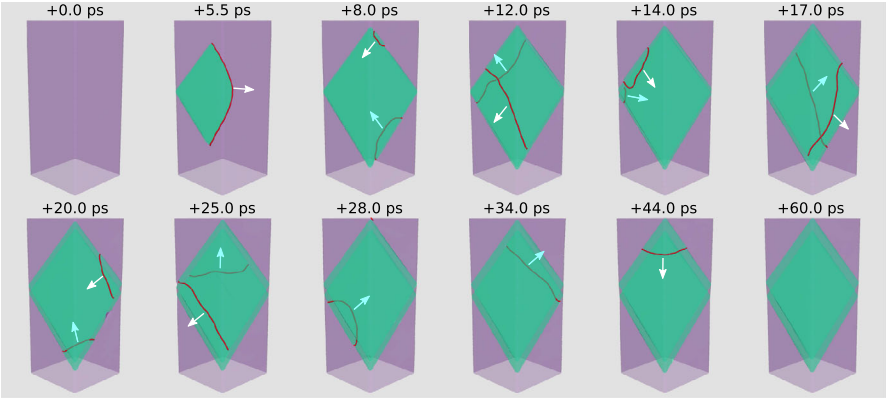

FIG. 1. DT initiation in a [100] oriented square Cu nanowire via surface rebound process. The starting time for DT initiation is 53.858 ns (i.e., +0.0 ps). Red lines are partial dislocation cores, green planes are stacking faults or twin boundaries and short arrows represent directions of dislocation motion.

nanowire under tensile loading. This fascinating observation invites two important questions. First, what is the physical origin of the observed surface rebound? Second, exactly how DT is initiated under typical laboratory and MD simulation conditions, i.e., is this SRS mechanism favored over the TAN mechanism? In what follows, we first rationalize the observed surface rebound and then elucidate the strongly correlated DT initiation process.

MD simulations showed that, under sufficiently high shear stress τ, dislocations can be accelerated to become [24], or even directly born as [25] "relativistic dislocations." As shown in Fig. 2, a partial dislocation was accelerated under an applied τ of 1.55 GPa (typical in laboratory experiments on dislocation-free samples [1,26]) at 2 K. Although being dragged by free surface, the front of a partial dislocation loop was still accelerated to a speed as high as $\sim 0.84 c_t$ and within a distance as short as ~20 nm. Phonon drag has minor effects on this acceleration [27]. As such, dislocations can conceivably enter the kinetic energy dominated, i.e., strongly overdriven, regime in highly stressed pristine crystals.

A dislocation becomes relativistic when the kinetic energy E_k associated with the core becomes equally important as the potential energy E_p ($E_{\text{core}} = E_p + E_k$), and no longer negligible for dislocation reactions [28–31]. When a dislocation with speed v hits a surface, E_{core} must dissipate into heat and transform into new defects (e.g., slip offset, point defects, and mostly M new dislocations). Energy conservation requires

$$E_p(v) + E_k(v) = E_{\text{config}} + \int R_D dt + H(v - v_c) \times \sum_{i=1}^{M} \int R_i dt, \quad (1)$$

where E_{config} is the potential energy of the local configuration due to dislocation annihilation (e.g., a surface slip step), R_D is the dissipation rate into heat, R_i is the transformation rate of E_{core} into the potential energy of ith dislocation, and $H(v - v_c)$ is the Heaviside step function to account for the sharp transition from annihilation to rebound once the dislocation speed v exceeds a critical value v_c.

For $v \ll v_c$, E_k is negligible and there is little new dislocation generation, so $E_{\text{core}} \sim E_p \sim E_{\text{config}} + \int R_D dt$, leading to normal annihilation. For $v > v_c$, the extra E_k feeds into $\int R_D dt + \sum_{i=1}^{M} \int R_i dt$ and the competition between R_D and R_i determines how the system evolves. In our model, defect generation is favored because it involves localized bond breaking which is more efficient than dissipation into heat via elastic bond vibrations, i.e.,$E_k \sim \sum_{i=1}^{M} \int R_i dt$. For a successful dislocation nucleation, the critical (saddle) configuration has to be reached, requiring $\sum_{i=1}^{M} \int R_i dt \geq \sum_{i=1}^{M} Q_i$, where Q_i is the activation barrier (free energy) for dislocation i. Thus for a single rebound, it is necessary that

$$E_k(v) \geq Q \quad \text{and} \quad R_1 \gg R_D. \quad (2)$$

This criterion suggests that once a dislocation accelerates to a critical speed such that its kinetic energy more than compensates for the Q of surface dislocation, the latter nucleates, provided that the dissipation of core energy into heat is insignificant over the very short time period for nucleation.

Our analyses based on the FENEB method and direct MD simulations lend support to Eq. (2). In Fig. 3, using a

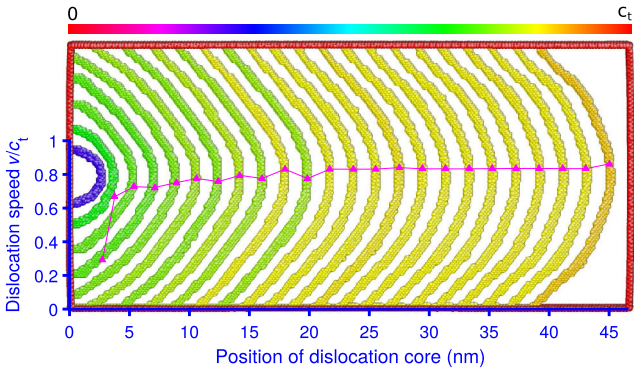

FIG. 2. Trajectory of a partial dislocation being accelerated in a copper slab subjected to a shear stress $\tau \sim 1.55$ GPa at 2 K. The dislocation line is colored corresponding to its instantaneous speed. The crystals directions are $[\bar{1}10]$, $[11\bar{2}]$, and [111] along the dislocation motion direction, the tangent of dislocation front and the slip plane normal.

copper slab under shear stresses τ, $E_k(\tau)$ is compared with the $Q_0(\tau)$, i.e., the Q at 0 K, of a twinning dislocation (after the first leading partial annihilates and leaves behind a stacking fault). In Fig. 3(a), the dislocation core carrying the necessary kinetic energy is identified using the common neighbor analysis (CNA) [32,33]. Atoms right above and below the CNA core are included [Fig. 3(b)] as the rebound process involves these two additional atomic layers. Such a choice of core region to evaluate the necessary E_k is based on the localized nature of dislocation nucleation at the site where a high-speed dislocation hits the surface [34]. $Q_0(\tau)$ is obtained using the FENEB method (see Ref. [35]). A typical saddle configuration for surface dislocation nucleation is shown in Fig. 3(c), which suggests an approximately semicircular shape involving two atomic planes. The results can be expressed as [Fig. 3(d)] $Q_0(\tau) = A\{1 - \exp[\alpha(1 - \tau/\tau_0)]\}$ [12], where A, α, and τ_0 are fitting parameters. This enables us to calculate the activation volume at different τ, from which we can estimate the corresponding incident dislocation length l_{inc} (i.e., the diameter of the semicircular saddle loop which is usually a few nanometers) involved in rebounding a new dislocation: $l_{\text{inc}} = 2[2(-\partial Q_0/\partial\tau)/(\pi a/\sqrt{3})]^{1/2}$, where a is the lattice constant. E_k is then evaluated for atoms inside the volume defined by l_{inc}, the core width, and core height [see the box in Fig. 3(b) and further explanation in Ref. [34]]. In Fig. 3(d), we see that $Q_0(\tau)$ and $E_k(\tau)$ intersect at $\tau \sim 1.45$ GPa, above which inequality (2) becomes satisfied. This critical τ for surface rebound to occur is consistent with the $\tau_{\text{reb}} \sim 1.4$ GPa, directly observed in our MD simulations. Figures 3(e) and 3(f) show the rebounded dislocation configurations under τ_{reb} and an initial temperature 2 K, which subsequently rose to ~12 K for a ~70 nm long incident dislocation. Viewed from the top [Fig. 3(e)] or bottom [Fig. 3(f)] in the direction along the dislocation line, the rebounded small dislocation loops alternate their locations from the upper layer to the lower layer, because near the critical τ_{reb} the E_k of the incident partial dislocation is sufficient to nucleate only one new partial, which emerges either above or below the original slip plane with apparently the same probability. Surface rebound was hypothesized by Frank [37] and Christian [38] before, but our MD simulations directly demonstrated it in a realistic metal and revealed its kinetic energy origin. Note that the typical artifacts associated with MD simulation of defect processes, those of unrealistically high applied strain rate and lack of rare-event sampling, are irrelevant here, since rebound arises only from an existing dislocation.

Next, we show that the SRS process is indeed the dominant mechanism to initiate DT in a copper nanowire, the sample geometry often used in laboratory experiments. The temporal correlation of dislocation dynamics in DT can be evaluated by the delay time t between two successive twinning dislocations, the nth after the $(n-1)$th. The shorter the t, the stronger the temporal correlation between the two. If the average t for SRS process t_{SRS} is significantly smaller than that of the TAN process t_{TAN}, i.e., $t_{\text{SRS}} \ll t_{\text{TAN}}$, then the SRS process would preempt the TAN. Here we evaluate the t_{SRS} by considering the travel distances and dislocation speeds for a 30 nm wide [100] oriented nanowire at 300 K. First, this nanowire is loaded under uniform compression to different σ levels at a strain rate of 10^8 s^{-1}. At each σ after relaxation, a small dislocation loop was introduced at one of the favored equivalent corners and accelerated to glide across the nanowire. By repeating such simulation under different σ,

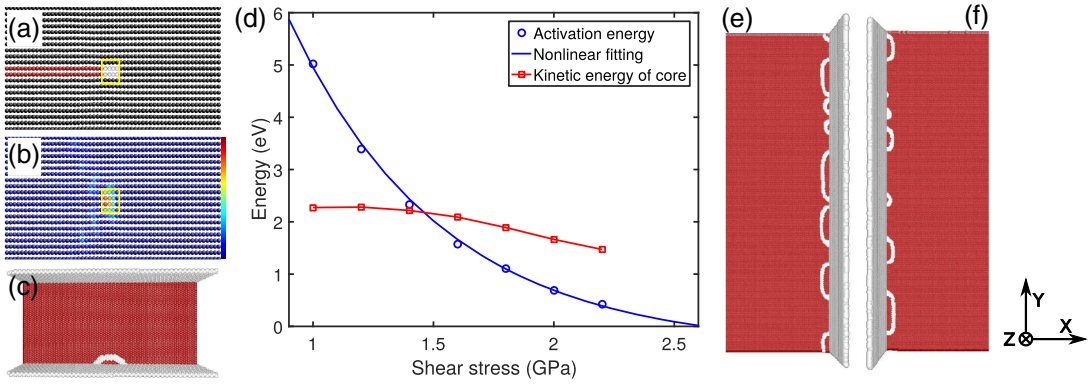

FIG. 3. Kinetic energy of the dislocation core induces free surface dislocation rebound. (a) The partial dislocation core (white atoms) identified by common neighbor analysis (CNA). (b) The core region (the yellow box) used in evaluating the kinetic energy. The color bar indicates the atomic kinetic energy range from 0 (blue) to 0.056 eV (red). (c) The saddle configuration of a twinning dislocation. The imposed shear stress τ in (a)–(c) is 1.6 GPa. (d) The kinetic energy of the dislocation core and the activation energy of twinning dislocation nucleation. (e)–(f) The rebounded dislocation loops of a ~70 nm long incident partial dislocation under the critical $\tau_{\text{reb}} = 1.4$ GPa at an initial temperature 2 K. The snapshots are taken at 1.3 ps after the impact. (a) and (b) share the same coordinate system: $X[1\bar{1}0]$, $Y[\bar{1}\,\bar{1}\,\bar{1}]$, and $Z[\bar{1}\,\bar{1}\,2]$. Coordinate systems in (c),(e), and (f) are $X[11\bar{2}]$, $Y[\bar{1}10]$, $Z[\bar{1}\,\bar{1}\,\bar{1}]$; $X[1\bar{1}0]$, $Y[\bar{1}\,\bar{1}\,2]$, $Z[111]$; and $X[\bar{1}10]$, $Y[\bar{1}\,\bar{1}\,2]$, $Z[\bar{1}\,\bar{1}\,\bar{1}]$, respectively. Atoms in (c), (e), and (f) are colored according to CNA. Red atoms represent stacking faults or twin boundaries, atoms on dislocation cores or free surfaces are white, and perfect FCC atoms are black.

the critical speed and axial stress for rebound in this nanowire was estimated to be $v_c \sim 0.60 c_t$ and $\sigma_{\text{reb}} \sim 1.5$ GPa, respectively. See Ref. [39] for typical rebound around the critical σ. Then t_{SRS} was estimated via dividing the characteristic sample length D (dislocation travel distance between two successive rebounds) by the dislocation speed v. This is because the frequency for SRS dislocations to hit the surface is very high in the nanoscale sample ($\sim 10^{10}$ s^{-1}, estimated from $v_c/10^2$ nm), and there is no time delay at the surfaces since Q is overcome entirely by E_k. The range of t_{SRS} (yellow band) by taking $v_c < v(\tau) < c_t$ and 10 nm $< D <$ 100 nm is shown in Fig. 4(a).

In comparison, for the TAN process the rate takes an Arrhenius form. Thus t_{TAN} can be calculated from the nucleation rate based on the activation free energy barrier Q. Here, $Q_0(\sigma)$ was FENEB calculated on the zero-T potential energy surface for the first six partial dislocations in a smaller ($\sim$5 nm wide) nanowire under different σ (see Ref. [40] for details). $Q(T) = (1 - T/T^*)Q_0(\sigma)$ [11] gives the value at $T = 300$ K, where $T^* = 700$ K is the approximate surface disordering temperature. t_{TAN} is then calculated according to $t_{\text{TAN}} = (\nu N)^{-1} \exp(Q/kT)$, where ν is the attempt frequency (3.0×10^{11} s^{-1}), N the total number of nucleation sites, and k the Boltzmann constant.

The results are shown in Fig. 4(a). In the limiting case where σ is so high that it overcomes the Q, TAN approaches the athermal limit such that the t_{TAN} of each partial becomes comparable with, or even shorter than, t_{SRS}. That is, when the σ level is initially very high prior to dislocation nucleation, TAN events could be too rampant on sample surfaces to leave any chance for the SRS process to operate. In our case, this happens [see the crossover in Fig. 4(a) of the t_{SRS} band with the t_{TAN} of the first couple of partial dislocations that initiate DT] when the axial stress $\sigma_{\text{ath}} \sim 2.75$ GPa at $T = 300$ K, well above that needed for rebound to occur ($\sigma_{\text{reb}} \sim 1.5$ GPa). As such, a wide stress window $[\sigma_{\text{reb}}, \sigma_{\text{ath}}]$ exists, where $t_{\text{SRS}} \ll t_{\text{TAN}}$. In this regime, the SRS dislocations easily preempt TAN due to their extraordinary temporal correlation. The $t_{\text{TAN}}(\sigma)$ curve would shift to the left with increasing twin thickness, but the driving stress level also gradually decreases such that the t_{TAN} remains well above t_{SRS}.

Figure 4(b) displays the axial stress σ_{p1} needed to nucleate the first dislocation via TAN, predicted based on the Q used in Fig. 4(a) at $T = 300$ K (see Ref. [41] for details of the calculation). The stress regime $[\sigma_{\text{reb}}, \sigma_{\text{ath}}]$ discussed above is indicated by the dashed lines. For normally accessible strain rates (from laboratory strain rate 10^{-3} s^{-1} to MD strain rates 10^8 s^{-1}), σ_{p1} almost perfectly falls into the stress window $[\sigma_{\text{reb}}, \sigma_{\text{ath}}]$, suggesting that when the first TAN event starts, the stress level is already sufficiently high for the SRS twinning dislocations to readily take over the subsequent DT initiation. This is consistent with our direct MD simulation shown in Fig. 1 where $\sigma_{p1} \sim 2.5$ GPa under the strain rate of 10^6 s^{-1} and DT is initiated completely by SRS twinning dislocations. On the contrary, as shown in Ref. [42], when a

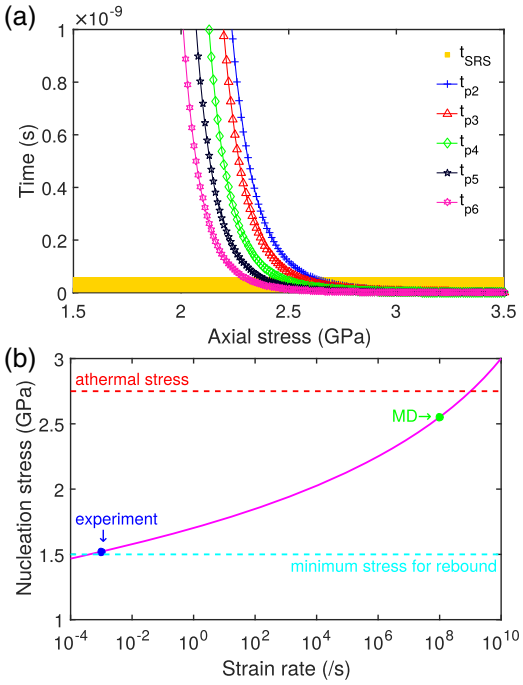

FIG. 4. Determination on the dominant mechanism underlying the strongly correlated DT initiation. (a) Delay time (or the temporal correlation) between successive dislocations. (b) The nucleation axial stress of the first dislocation via TAN at 300 K for normally accessible strain rates (as marked in the figure, 10^{-3} s^{-1} is typical for the strain rates used in laboratories, and 10^8 s^{-1} is often the strain rate applied in MD simulations), the predicted nucleation axial stress falls in the range of [1.5 GPa, 2.75 GPa] within which $t_{\text{SRS}} \leq t_{\text{TAN}}$.

50 nm NW is compressed under a much higher strain rate 10^9 s^{-1} at $T = 300$ K, σ_{p1} now becomes $\sim$3.0 GPa and TAN overwhelmingly dominates DT initiation. The above SRS dominated twinning stress window, on the order of 10^{-2} G, is encountered in laboratory experiments on most nanoscale metals such as Au [2,4], Cu [1,26,43], Al [44], Pd [3,5,45], and Ni [46], where the sample-level σ reported to nucleate the first dislocation is usually well in excess of 10^{-2} G, in the so-called ultra-strength regime [47,48]. We therefore conclude that SRS twinning dislocations constitute the preferred mechanism over TAN to initiate DT in typical small-volume experiments.

In summary, partial dislocations nucleated on the surface of pristine crystals can be accelerated by high stresses to approach the speed of the shear wave within a distance as short as 10^1 nm, and "bounce" back at free surfaces as twinning dislocations, directly initiating DT in a highly correlated, domino cascade manner. We confirmed that such surface rebound is a consequence of a strongly overdriven dislocation core carrying sufficiently high kinetic energy to overcome the static nucleation energy barrier of new dislocations. From the delay time to generate the next twinning dislocation, the surface rebound mechanism is significantly more probable than the TAN process under the same loading conditions. For a wide range of strain rates, the

nucleation stress of the first partial dislocation in metallic nanowires is well beyond the minimum stress required for surface rebound. These render the surface rebound mechanism highly efficient and preferable. As such, in an experimentally relevant stress window, SRS relay dominates over TAN for DT initiation. This affirms the nature of DT to be "stimulated slip," and its strongly correlated kinetics *vis-à-vis* ordinary dislocation slip is akin to "what laser (light amplification by stimulated emission of radiation) is to normal light" [49]. In DT-SRS the stimulation is of kinetic energy origin, whereas in DT-TAN (below σ_{reb} or above σ_{ath}) the stimulation is of configurational energy origin.

Note that a nanoscale pristine crystal is only one example that is amenable to the operation of surface rebound. The mechanism demonstrated here may also have relevance to high-stress or high-strain-rate deformation in general, where strongly overdriven dislocations interact with interfaces. For example, DT in bulk nanocrystalline metals relies on partials nucleated from grain boundaries under high stresses to run towards opposing boundaries at high speeds. In shock loading, the shock width is too small to include many dislocation sources, such that high-speed dislocation interacting with large voids [50] or phase boundaries [51] may come into play to multiply dislocations.

Q. J. L. and E. M. were supported by U.S.-DOE-BES-DMSE, DE-FG02-09ER46056. J. L. acknowledges support by NSF Grant No. DMR-1410636. Z. W. S. was supported by NSFC Grants No. 51231005, No. 51321003 and the International Joint Laboratory for Micro/Nano Manufacturing and Measurement Technologies.

*Corresponding authors.
liju@mit.edu
†zwshan@mail.xjtu.edu.cn
‡ema@jhu.edu

[1] G. Richter, K. Hillerich, D. S. Gianola, R. Mönig, O. Kraft, and C. A. Volkert, Nano Lett. **9**, 3048 (2009).
[2] J.-H. Seo *et al.*, Nano Lett. **11**, 3499 (2011).
[3] L. Y. Chen, G. Richter, J. P. Sullivan, and D. S. Gianola, Phys. Rev. Lett. **109**, 125503 (2012).
[4] A. Sedlmayr, E. Bitzek, D. S. Gianola, G. Richter, R. Mönig, and O. Kraft, Acta Mater. **60**, 3985 (2012).
[5] J.-H. Seo, H. S. Park, Y. Yoo, T.-Y. Seong, J. Li, J.-P. Ahn, B. Kim, and I.-S. Choi, Nano Lett. **13**, 5112 (2013).
[6] B. Roos, B. Kapelle, G. Richter, and C. A. Volkert, Appl. Phys. Lett. **105**, 201908 (2014).
[7] L. Y. Chen, M.-r. He, J. Shin, G. Richter, and D. S. Gianola, Nat. Mater. **14**, 707 (2015).
[8] See Supplemental Material at http://link.aps.org/supplemental/10.1103/PhysRevLett.117.165501, Fig. S1, for the schematic of strongly correlated deformation twinning initiation process, which includes Refs. [2, 4–6].
[9] A. H. Cottrell and B. A. Bilby, Philos. Mag. **42**, 573 (1951).
[10] N. Thompson and D. J. Millard, Philos. Mag. **43**, 422 (1952).
[11] T. Zhu, J. Li, A. Samanta, A. Leach, and K. Gall, Phys. Rev. Lett. **100**, 025502 (2008).
[12] C. R. Weinberger, A. T. Jennings, K. Kang, and J. R. Greer, J. Mech. Phys. Solids **60**, 84 (2012).
[13] A. T. Jennings, C. R. Weinberger, S.-W. Lee, Z. H. Aitken, L. Meza, and J. R. Greer, Acta Mater. **61**, 2244 (2013).
[14] T. Zhu, J. Li, A. Samanta, H. G. Kim, and S. Suresh, Proc. Natl. Acad. Sci. U.S.A. **104**, 3031 (2007).
[15] Y. Mishin, M. J. Mehl, D. A. Papaconstantopoulos, A. F. Voter, and J. D. Kress, Phys. Rev. B **63**, 224106 (2001).
[16] S. Plimpton, J. Comput. Phys. **117**, 1 (1995).
[17] J. Li, Model. Simul. Mater. Sci. Eng. **11**, 173 (2003).
[18] A. Stukowski and K. Albe, Model. Simul. Mater. Sci. Eng. **18**, 085001 (2010).
[19] See Supplemental Material at http://link.aps.org/supplemental/10.1103/PhysRevLett.117.165501, section II, for more details on simulation methods, which includes Ref. [20].
[20] M. Parrinello and A. Rahman, J. Appl. Phys. **52**, 7182 (1981).
[21] See Supplemental Material at http://link.aps.org/supplemental/10.1103/PhysRevLett.117.165501, Fig. S2, for the stress vs time curve for the 10 nm wide nanowire being compressed.
[22] See Supplemental Material at http://link.aps.org/supplemental/10.1103/PhysRevLett.117.165501, movie 1, for the surface rebound sustained deformation twinning initiation as discussed in Fig. 1 in text.
[23] See Supplemental Material at http://link.aps.org/supplemental/10.1103/PhysRevLett.117.165501, movie 2, for surface rebound dominated DT initiation in a 10 nm wide [110] oriented nanowire under tensile loading.
[24] L. O. David, G. H. Louis, Jr., W. A. Curtin, and R. J. Clifton, Model. Simul. Mater. Sci. Eng. **13**, 371 (2005).
[25] P. Gumbsch and H. Gao, Science **283**, 965 (1999).
[26] D. Kiener and A. M. Minor, Nano Lett. **11**, 3816 (2011).
[27] See Supplemental Material at http://link.aps.org/supplemental/10.1103/PhysRevLett.117.165501, Fig. S3, for a dislocation acceleration process at 300 K.
[28] J. D. Eshelby, Proc. Phys. Soc. London Sect. A **62**, 307 (1949).
[29] F. C. Frank, Proc. Phys. Soc. London Sect. A **62**, 131 (1949).
[30] J. Weertman, in *Response of Metals to High Velocity Deformation*, edited by P. G. Showmon and V. F. Zackay (Interscience, New York, Colorado, 1961), p. 205.
[31] J. Hirth and J. Lothe, *Theory of Dislocations*, 2nd ed. (John Wiley & Sons, New York, 1982).
[32] D. Faken and H. Jónsson, Comput. Mater. Sci. **2**, 279 (1994).
[33] H. Tsuzuki, P. S. Branicio, and J. P. Rino, Comput. Phys. Commun. **177**, 518 (2007).
[34] See Supplemental Material at http://link.aps.org/supplemental/10.1103/PhysRevLett.117.165501, Fig. S4, Fig. S5, Fig. S6 and associated discussions, for the underlying physics for choosing the core region to calculate the effective kinetic energy during the surface rebound process.
[35] See Supplemental Material at http://link.aps.org/supplemental/10.1103/PhysRevLett.117.165501, section II and Fig. S7, for details on the free end nudged elastic band calculations, which includes Refs. [11,14,36].
[36] G. Henkelman and H. Jónsson, J. Chem. Phys. **111**, 7010 (1999).
[37] F. C. Frank, *Report of the Conference on Strength of Solids* (Physical Society, London, Bristol, 1948), p. 46.

[38] J. W. Christian, Proc. R. Soc. A **206**, 51 (1951).
[39] See Supplemental Material at http://link.aps.org/supplemental/10.1103/PhysRevLett.117.165501, Fig. S8, for typical DT initiation processes in a 30 nm nanowire with axial stress around the critical value for surface rebound.
[40] See Supplemental Material at http://link.aps.org/supplemental/10.1103/PhysRevLett.117.165501, section II and Fig. S9, for details on free end nudged elastic band calculations on the activation energies of the first six partial dislocations during deformation twinning initiation in a nanowire.
[41] See Supplemental Material at http://link.aps.org/supplemental/10.1103/PhysRevLett.117.165501, section II, for more details on the nucleation stress calculations.
[42] See Supplemental Material at http://link.aps.org/supplemental/10.1103/PhysRevLett.117.165501, movie 3, for thermally activated nucleation dominated deformation twinning initiation in a 50 nm wide nanowire compressed to near the athermal stress level.
[43] Y. Yue, P. Liu, Z. Zhang, X. Han, and E. Ma, Nano Lett. **11**, 3151 (2011).
[44] Z.-J. Wang, Q.-J. Li, Z.-W. Shan, J. Li, J. Sun, and E. Ma, Appl. Phys. Lett. **100**, 071906 (2012).
[45] L. Y. Chen, S. Terrab, K. F. Murphy, J. P. Sullivan, X. Cheng, and D. S. Gianola, Rev. Sci. Instrum. **85**, 013901 (2014).
[46] C. Peng, Y. Ganesan, Y. Lu, and J. Lou, J. Appl. Phys. **111**, 063524 (2012).
[47] T. Zhu and J. Li, Prog. Mater. Sci. **55**, 710 (2010).
[48] J. Li, Z. Shan, and E. Ma, MRS Bull. **39**, 108 (2014).
[49] Q. Yu, Z.-W. Shan, J. Li, X. Huang, L. Xiao, J. Sun, and E. Ma, Nature (London) **463**, 335 (2010).
[50] L. Xiong, S. Xu, D. L. McDowell, and Y. Chen, Int. J. Plast. **65**, 33 (2015).
[51] P. A. Pluchino, X. Chen, M. Garcia, L. Xiong, D. L. McDowell, and Y. Chen, Comput. Mater. Sci. **111**, 1 (2016).

Supplementary Materials for

Surface rebound of relativistic dislocations directly and efficiently initiates deformation twinning

Qing-Jie Li[1], Ju Li[2], Zhi-Wei Shan[3], Evan Ma[1]

[1]*Department of Materials Science and Engineering, Johns Hopkins University, Baltimore, Maryland 21218, USA*

[2]*Department of Nuclear Science and Engineering and Department of Materials Science and Engineering, Massachusetts Institute of Technology, 77 Massachusetts Avenue, Cambridge, Massachusetts 02139, USA*

[3]*Center for Advancing Materials Performance from the Nanoscale (CAMP-Nano) & Hysitron Applied Research Center in China (HARCC), State Key Laboratory for Mechanical Behavior of Materials, Xi'an Jiaotong University, Xi'an 710049, China.*

Correspondence should be addressed to: J. Li liju@mit.edu or Z.W. Shan zwshan@gmail.com or E. Ma ema@jhu.edu

1. Extremely stringent spatial-temporal correlation between twinning dislocations

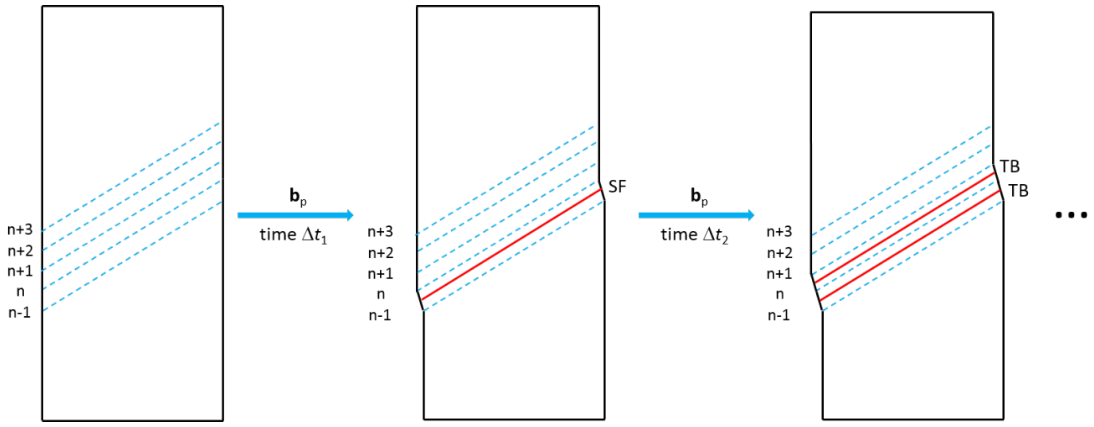

Fig. S1. Schematic of strongly correlated deformation twinning (DT) initiation. The first partial dislocation with Burgers vector $\mathbf{b}_p$ nucleates on the n^{th} atomic layer. Then a twinning dislocation with the same Burgers vector $\mathbf{b}_p$ has to nucleate on either the $(n\text{-}1)^{th}$ or $(n\text{+}1)^{th}$ atomic layer (the above schematic shows a twinning dislocation on the $(n\text{+}1)^{th}$ layer). Similar nucleation process should be repeated stringently on successive atomic layers. Furthermore, for the experimentally observed transient DT initiation process [2,4-6], the delay time between two successive twinning dislocations Δt_i has to be very small as well.

2. Simulation details and supplementary figures

- **Compression of copper nanowire (Fig. 1 in text)**

  A 10 nm wide square nanowire was constructed with periodic boundary conditions along the axial direction [100] and free surfaces in the other two directions [010] and [001], respectively. Then the nanowire was equilibrated at 300 K for 20 ps under NPT conditions with pressure in the axial direction kept at 0 GPa. Temperature was controlled by Nose-Hoover thermostat and pressure was controlled via the Parrinello-Rahman method [50]. Afterwards, the nanowire was compressed with a strain rate of 10^6 s^{-1} and both the thermostat and barostat were turned off. Fig. S2 shows the axial stress vs. time curve.

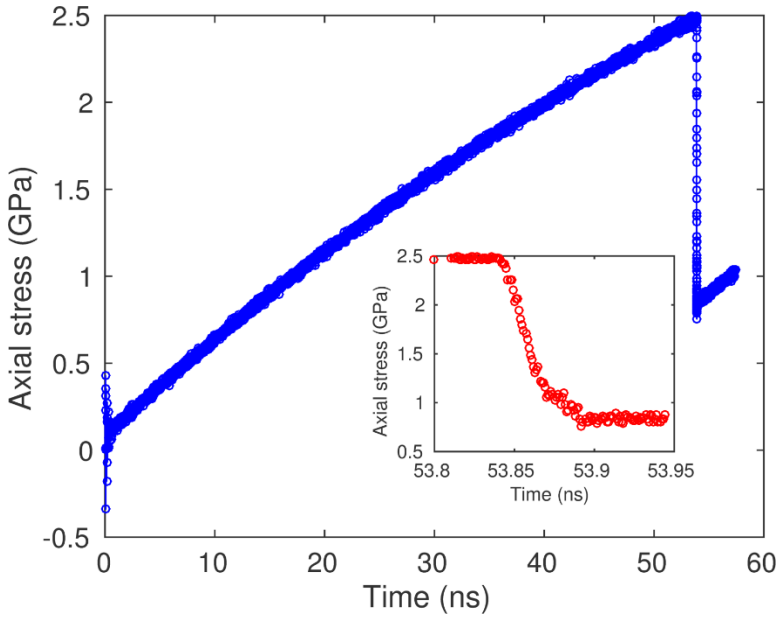

Fig. S2. Axial stress vs. time for the 10 nm wide nanowire during compression at the strain rate of 10^6 s^{-1}. The inset shows the stress drop during DT initiation which is accomplished within ~60 ps.

- **Acceleration of partial dislocation (Fig. 2 in text)**

  Free surfaces were used in all three directions and the sample size was 46 nm × 15 nm × 28 nm. The system was first equilibrated at T = 2 K or T = 300 K for 20 ps. Temperature was controlled by Nose-Hoover thermostat. Then a shear stress τ_{yz} was ramped to the desired stress level by gradually adding a z force component to atoms on surfaces perpendicular to the y direction. After the shear stress reached the constant value, dislocations were "nucleated" by rigidly shifting some atoms below and above the slip plane within a very short time (< 1 ps). The nucleated dislocation was then accelerated under the applied shear stress. Dislocation speed was calculated by measuring the dislocation core position at different time. Fig. S3 shows an acceleration process at 300 K.

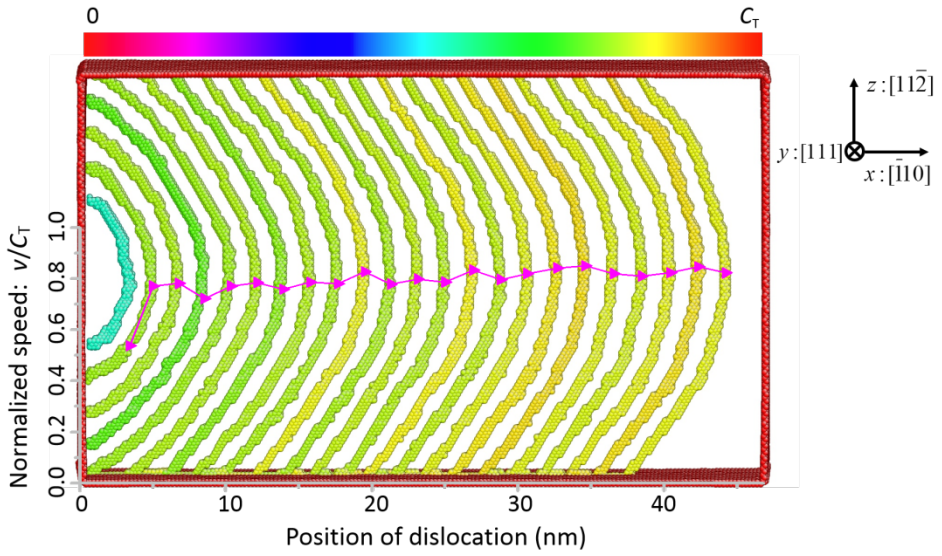

Fig. S3. The acceleration process of a "nucleated" partial dislocation in copper under an applied shear stress τ = 1.35 GPa at 300 K. The acceleration parameters such as the acceleration distance (tens of nanometers) and the steady-state speed reached (~0.82c_t) have not changed too much from that presented in Fig. 2 in text for T = 2 K.

- **Validation of Inequality (2) in text (Fig. 3 in text)**

  In all simulations including calculation on kinetic energy of core, activation energy barriers from free end nudged elastic band (FENEB) method [11,14] and MD simulations on surface rebound, periodic boundary conditions were imposed along the dislocation line direction $[11\bar{2}]$ and the normal direction of the [111] slip plane. Free surface was used along the dislocation glide direction $[1\bar{1}0]$. The sample size used was $[1\bar{1}0]$ 61 nm × [111] 75 nm × $[11\bar{2}]$ 3.5 nm for calculating the kinetic energy, $[1\bar{1}0]$ 61 nm × [111] 18 nm × $[11\bar{2}]$ 71 nm for observing the critical shear stress for rebound at a flat surface and $[1\bar{1}0]$ 10.2 nm × [111] 7.5 nm × $[11\bar{2}]$ 21.3 nm for FENEB calculations. In simulations on calculating kinetic energy and observing critical shear stress for rebound, both temperatures were initially set to ~2 K and not controlled during the motion of the dislocation to avoid interrupting the core energy. Pressure was controlled by Parrinello-Rahman [50] methods. After equilibrated at the initial temperature and pressure for 20 ps, a dislocation was introduced at the left surface and accelerated to glide towards the opposite surface.

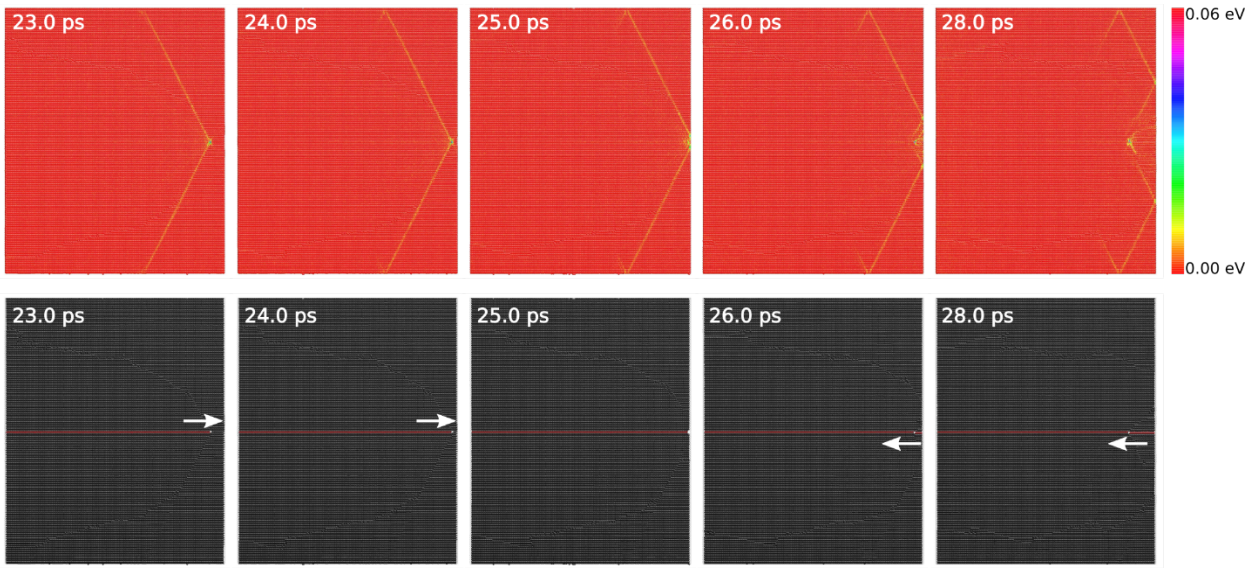

Fig. S4. Atomic kinetic energy distribution during surface rebound process. The bottom panels show the corresponding dislocation core and stacking fault/twin boundary identified by the common neighbor analysis (CNA). The applied shear stress is 1.45 GPa and initial temperature is ~2.5 K.

Fig. S4 shows the underlying physics for calculating the effective kinetic energy (the kinetic energy of atoms contained in the box as shown in Fig. 3 of the text) that triggers surface dislocation rebound. The full kinetic energy of a moving dislocation can be treated using the concept of effective mass: $E(v) = E_0 + 1/2m^*v^2$, where $E(v)$ is the total energy of the moving dislocation, E_0 is the rest energy of the dislocation, v is the velocity of the moving dislocation and $m^*=E_0/(c_t)^2$ is the effective mass of the moving dislocation. The second term in the above equation is defined as the full kinetic energy associated with the moving dislocation, which actually includes the excess potential energy (difference of atomic potential energy of a moving dislocation and a static dislocation) and kinetic energy of the atoms in the core region and in the elastic field of the moving dislocation. The atomic kinetic energy (kinetic energy due to dislocation motion and temperature which however is negligible in our case) distribution in a crystal containing a moving partial dislocation is shown in Fig. S4. As can be seen in the upper panels of Fig. S4, the atomic kinetic energy distribution (i.e., the "Mach-cone-like" profile) due to a moving partial dislocation generally spreads over the entire crystal and

the total kinetic energy of a moving dislocation should be the full kinetic energy of the crystal minus the kinetic energy related to temperature. However, during the surface rebound process (i.e., from 24.0 ps to 26.0 ps in Fig. S4), only the kinetic energy around the atomistic dislocation core transformed into the new nucleating dislocation and the rest of the kinetic energy is simply reflected back and gradually dissipated (as can be seen in Fig. S4 from 25.0 ps to 28.0 ps, most of the boundary of the "Mach-cone-like" profile did not simply disappear but directly reflected back without generating new dislocations). This indicates that it should be the kinetic energy associated with the atoms at the core, rather than the entire kinetic energy spreading over the elastic field of a moving dislocation, that is responsible for forming the dislocation loop corresponding to the saddle point (energy barrier). This is also the physical origin of the strong spatial correlation of surface rebound: the most probable site for new dislocation generation during surface rebound is localized near the annihilation site of the incident dislocation rather than distributed in multiple places along the surface where the kinetic energy field of the incident dislocation is reflected. Furthermore, such a picture is consistent with the physics that surface dislocation nucleation is generally a heterogeneous event dominated by local conditions such as surface steps, stress concentrations, etc. Therefore, the choice of kinetic energy around the core region is based on the localized nature of dislocation nucleation when a high-speed dislocation hits the surface. As for the specific shape of the core region, here we identified it via the common neighbor analysis and took into account the extra atomic layers that were involved in the rebound dislocation. To reiterate, the above picture/rationale is aimed at representing the localized event of nucleating a critical-sized new dislocation at the site where the high-speed dislocation collides with surface, rather than for describing dislocation reactions on the continuum level (then one may instead consider the full kinetic energy associated with the effective mass of a moving dislocation, to balance with the elastic field energy of a rebounded and fully developed dislocation near surface).

To further support the above analysis, we also calculated the kinetic energy as a function of dislocation core size and analyzed the detailed surface rebound process. As shown in Fig. S5, the full kinetic energy and the kinetic energy due to moving dislocation

(full kinetic energy – kinetic energy due to temperature) generally increase with the size of the core region selected (the kinetic energy due to moving dislocation increases much more slowly at larger core sizes). Both kinds of kinetic energy do not converge as the dislocation elastic field and the profile of kinetic energy distribution can be infinitely large. At smaller sizes (below core 3; i.e., dislocation core ID 3), the full kinetic energy and kinetic energy due to dislocation motion are almost indistinguishable.

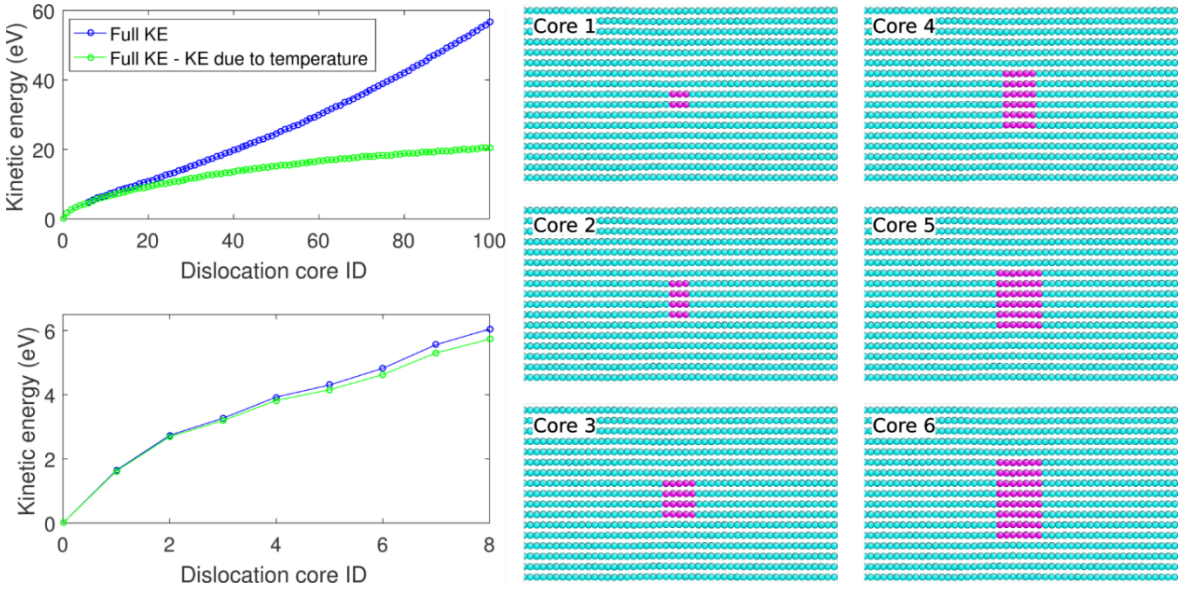

Fig. S5. The kinetic energy of dislocation core as a function of the core size selected. The lower-left plot is a local magnification of the upper-left plot. On the right, the first six cores with increasing sizes are shown. Specifically, the first core is the core identified by the common neighbor analysis (CNA); the second core is used in our current work.

Because the kinetic energy of dislocation core generally does not converge with increasing core sizes, one has to choose an appropriate core size to calculate the kinetic energy needed to nucleate new dislocations, based on the detailed physics of the surface rebound process. A detailed surface rebound process at 1.45 GPa and ~ 2.5 K is shown in Fig. S6. The typical surface rebound process can be described in four states, i.e., the initial state associated with the incoming dislocation core (24.4 ps), the annihilation state with a stacking fault left behind (24.8 ps), the localized activated complex state (25.1 ps), the new partial dislocation being rebounded (25.5 ps). Among these four states, the localized activated complex state is critical for the subsequent rebounded partial

dislocation. The atoms (red atoms) associated with this activated states are largely localized in the region bounded by the designated CNA core width and a height that is twice the CNA core width. This state needs to be reached, activated by the local atomic kinetic energies. As shown in the lower panel of Fig. R2, the atomic kinetic energy within a similar sized region (24.4 ps) of the incoming dislocation state was indeed significantly reduced when the activated state is reached (25.1 ps), suggesting that this is the size of the core in which the kinetic energy was transformed into the potential energy of the activated state. In other words, this is the appropriate size of the core to analyze the nucleation of rebound dislocations. Therefore, we chose the core size (CNA width × twice CNA height) that is similar to the size of the region of red atoms in the activated state to calculate the kinetic energy.

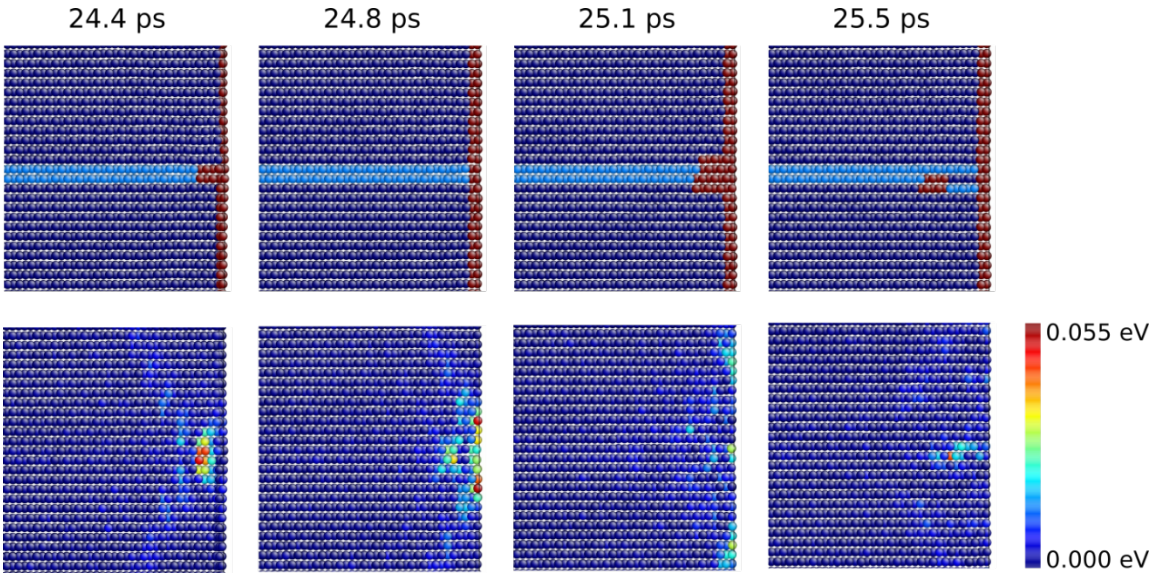

Fig. S6. A detailed surface rebound process at 1.45 GPa and ~ 2.5 K. Four important states are shown, i.e., the incoming partial dislocation, the annihilation state, the activated complex state and the rebounded partial dislocation. Dark blue atoms are FCC atoms, light blue atoms are HCP atoms and red atoms belong to not well defined structures. The corresponding atomic kinetic energy distribution are shown in the lower panel.

For FENEB calculations, the sample was pre-strained to different shear stress levels by applying a small increment shear strain each time and followed by an energy minimization via conjugate gradient method. Then at each chosen shear stress, a tentative

final state dislocation loop was created by a consecutive cut-displace-relax procedure. These tentative final states are chosen such that their potential energies are 0.1 - 0.3 eV lower than that of the initial states. Sixteen replicas are used along the reaction pathway for each FENEB calculation. The quickmin algorithm [51] was used to update atomic positions. Calculations are considered to be converged when the force on each replica is below 0.01 eV/Angstrom or the calculation step exceeds a rather large number (100,000 steps) such that the activation energy has a very small fluctuation. An example energy vs. reaction coordinate curve for the configuration given in Fig. 3(c) is shown in Fig. S5.

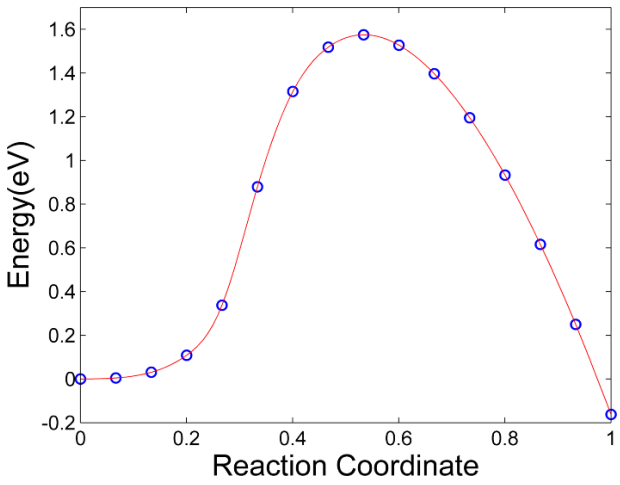

Fig. S7. The energy vs. reaction coordinate curve for the nucleation process in Fig. 3(c) at $\tau = 1.6$ GPa. The activation barrier height at the saddle point is ~1.6 eV. The saddle point configuration is shown in Fig. 3(c) of the main text.

- **Delay time and nucleation stress calculation (Fig. 4 in text)**

The critical speed and critical axial stress for surface rebound in a nanowire were determined using a similar configuration as that in Fig. 1 in text except that the width becomes 30 nm. Periodic boundary conditions were imposed along the nanowire axial direction and free surfaces in lateral directions. After relaxation for 20 ps at the initial temperature, the nanowire was compressed with a strain rate of $\sim 10^8$ s^{-1} to different stress levels. Then the configurations, taken out at a specific stress level, were relaxed (with the corresponding strain fixed) for 20 ps, and used to observe DT initiation via dislocation rebound. Dislocations were "nucleated" by rigidly shifting local atoms around the nanowire corner. Temperature were only initialized and not controlled by any thermostat.

Both initial 2 K and 300 K were tried. In all our MD simulations, the time step was set to 1 fs. Two examples of DT initiation by surface rebound are shown in Fig. S6.

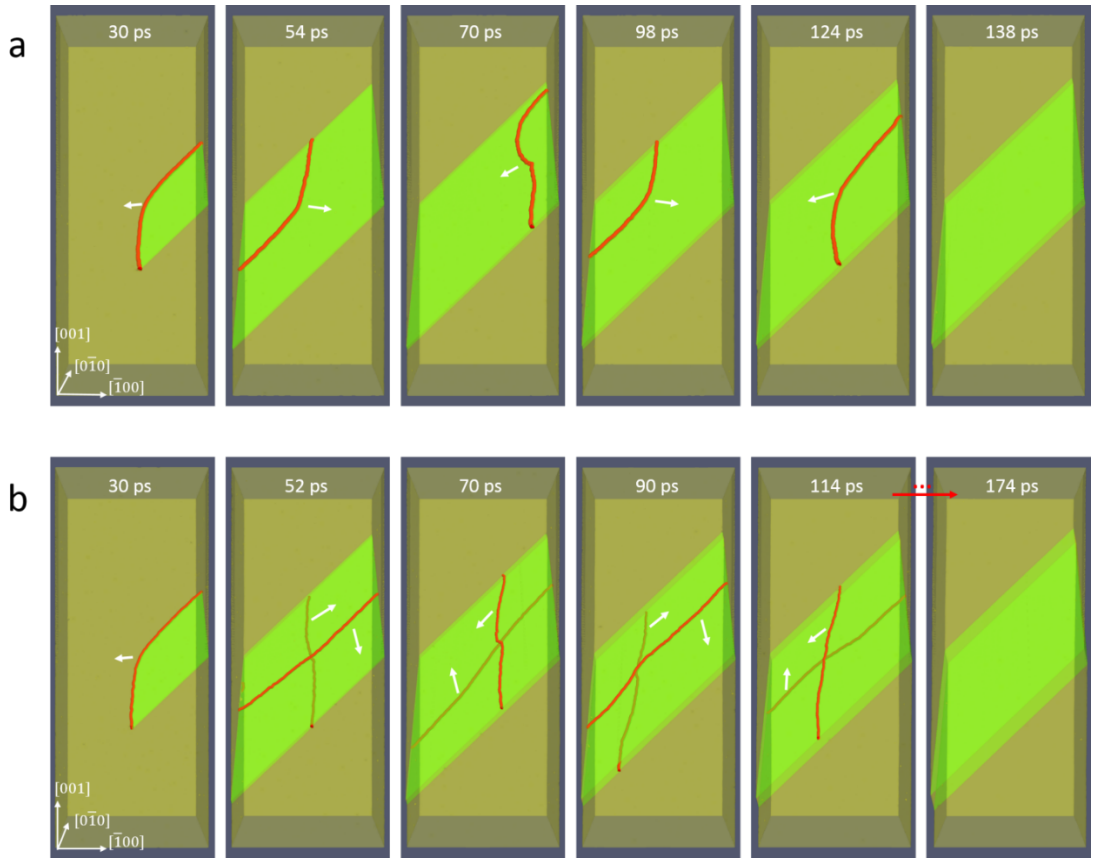

Fig. S8. DT initiation via surface dislocation rebound in a 30 nm wide copper nanowire at the initial temperature of 300 K. (a) DT initiated by single partial dislocation rebound with the initial axial stress $\sigma \sim$ 1.7 GPa. A $(111)\frac{1}{6}[11\bar{2}]$ dislocation was "nucleated" by rigidly shifting some local atoms at a corner. This leading partial dislocation then glides towards the opposite free surface (30 ps) and then rebounds back as a twinning dislocation on the neighboring slip plane (54 ps), forming a two-layer DT embryo. The ensuing rebounds repeatedly generate twinning partials (see the red gliding dislocation line at 70ps, 98ps and 124 ps), leading to a five-layer twin at 138 ps. (b) DT initiated by double partial dislocation rebound with the initial axial stress $\sigma \sim$ 1.94 GPa. The same leading partial dislocation rebounds back as two twinning dislocations on adjacent planes (52 ps), forming a three-layer DT. These two rebounded dislocations continue to rebound but on their opposite twin boundary respectively. Such rebounds repeat (see, e.g., 70 ps,

114 ps …). Finally, a thirteen-layer DT is formed (174 ps). Red lines delineate dislocation cores; translucent green layers are stacking faults or twin boundaries. White arrows indicate the glide direction of dislocations.

The activation energy barriers for the first six partial dislocations during DT initiation in a nanowire were calculated using a sample with dimensions of 5.24 nm × 5.24 nm × 11.57 nm. Periodic boundary conditions are imposed along the axial direction (with length 11.57 nm). The sample is pre-strained to different compressive stress levels by applying a small increment of compressive strain each time and followed by an energy minimization via conjugate gradient method. Then at each chosen stress level, a final configuration was obtained by nucleating a screw-like dislocation loop at one of the corners. The energies of these final configurations are usually 0.1 - 0.3 eV lower than that of the initial state. Eight replicas were used for each FENEB calculation. The quickmin algorithm [51] was used to update atomic positions. Calculations are considered to be converged when the force on each replica is below 0.01 eV/Angstrom or the calculation step exceeds a rather large number (100,000 steps) such that the activation energy has a very small fluctuation. Fig. S7 shows the activation energies.

The delay time between two successive twinning partials via thermally activated nucleation is calculated according to $t_{\mathrm{TAN}} = \frac{1}{\nu}\exp\left(\frac{Q}{kT}\right)$, where $Q = \left(1 - \frac{T}{T^*}\right)Q_0$ is the activation free energy at temperature T. Q_0 are the activation free energies at 0 K as shown in Fig. S7. Here the next partial dislocation is assumed to nucleate at a site next to that of the previous partial. The attempt frequency is $\nu = 3.1\times10^{11}$ s^{-1} [11].

The nucleation axial stresses for the first partial dislocation (σ_{p1}) under different strain rates at 300 K were obtained by numerically solving $\frac{Q(\sigma)}{kT} = \ln\frac{kTN\nu}{E\dot{\varepsilon}\Omega(\sigma)}$ [11], where $\Omega(\sigma)$ is the activation volume, E is the Young's modulus which is estimated to be ~ 61 GPa from molecular statics, N is the number of nucleation sites which is ~1,760 for the NW shown in Fig. S6 (only corner sites are counted, ~220 atoms on each corner and there are two equivalent slip systems for each atom, so N = 220 × 4 × 2.

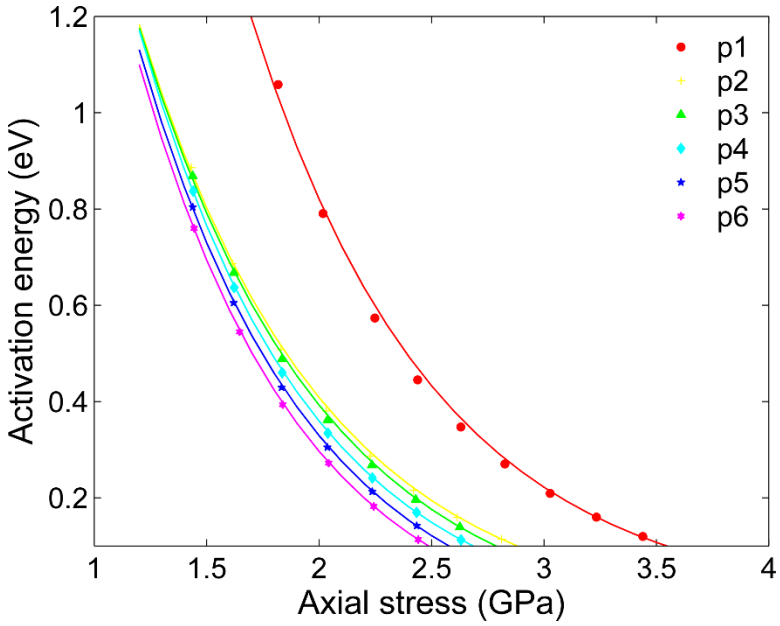

Fig. S9. Activation energies from FENEB calculations for the nucleation of the leading partial (red) and subsequent twinning partials. The activation barriers for each of these six partial dislocations (p1 through p6 on consecutive atomic planes) is shown as a function of the axial stress σ.

3. Supplementary Movies

Movie 1. Strongly correlated DT initiation in a 10 nm wide [100] oriented nanowire compressed with the strain rate of 10^6 s^{-1} at 300 K. The nucleation stress of the first partial dislocation is ~ 2.5 GPa and the DT initiation process is dominated by surface rebound sustained twinning dislocations.

Movie 2. Surface rebound dominated DT initiation in a 10 nm wide [110] oriented nanowire under tensile loading. The nanowire has a hexagonal cross-section and was first loaded up to ~4.7 GPa with the strain rate of 10^8 s^{-1} at 2 K. Then the nanowire was kept at the current strain and a small dislocation loop was introduced at one of the corners. The introduced dislocation then accelerated and induced more and more twinning dislocations. Similar scenarios have been observed under different axial stress levels.

Movie 3. DT initiation in 50 nm wide nanowire at a higher strain rate of 109 s-1 at 300 K. The nucleation stress of the first partial dislocation is ~ 3.0 GPa (close to the athermal limit) and DT initiation is dominated by the thermally activated nucleation of twinning dislocations.